High-Temperature Polaritons in Ceramic Nanotube Antennas
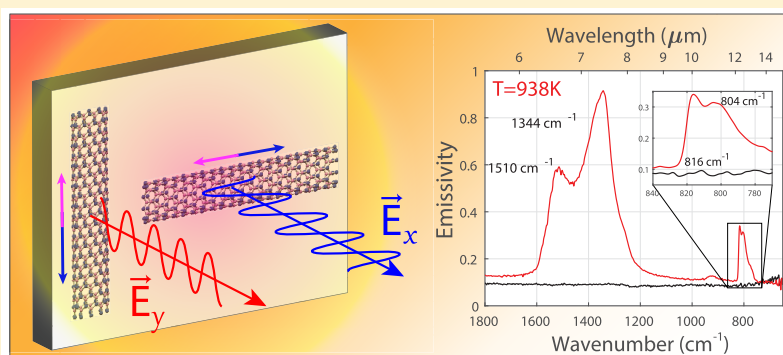
Ryan Starko-Bowes,[†] Xueji Wang,[‡] Zhujing Xu,[‡] Sandipan Pramanik,[†] Na Lu,[‡] Tongcang Li,[‡] and Zubin Jacob*,[‡,†]

[†]University of Alberta, Edmonton, Alberta T6G 2R3, Canada
[‡]Birck Nanotechnology Center, Purdue University, West Lafayette, Indiana 47907, United States

S *Supporting Information*

ABSTRACT: High-temperature thermal photonics presents unique challenges for engineers as the database of materials that can withstand extreme environments are limited. In particular, ceramics with high temperature stability that can support coupled light-matter excitations, that is, polaritons, open new avenues for engineering radiative heat transfer. Hexagonal boron nitride (hBN) is an emerging ceramic 2D material that possesses low-loss polaritons in two spectrally distinct mid-infrared frequency bands. The hyperbolic nature of these frequency bands leads to a large local density of states (LDOS). In 2D form, these polaritonic states are dark modes, bound to the material. In cylindrical form, boron nitride nanotubes (BNNTs) create subwavelength particles capable of coupling these dark modes to radiative ones. In this study, we leverage the high-frequency optical phonons present in BNNTs to create strong mid-IR thermal antenna emitters at high temperatures (938 K). Through direct measurement of thermal emission of a disordered system of BNNTs, we confirm their radiative polaritonic modes and show that the antenna behavior can be observed even in a disordered system. These are among the highest-frequency optical phonon polaritons that exist and could be used as high-temperature mid-IR thermal nanoantenna sources.

KEYWORDS: *Thermal emission, boron nitride nanotubes, phonon polaritons, nanoantenna, thermal photonics, high temperature radiator*

The field of thermal photonics aims to control the radiation emitted by objects due to thermal fluctuations within the medium. The field has experienced renewed interest due to the promise of emerging technologies such as thermophotovoltaics[1−4] and passive radiative cooling.[5,6] By careful consideration of an objects material composition as well as its micro/nanostructure, studies have shown it is possible to control spectrum, polarization, coherence and directionality of thermal radiation. The subset of high-temperature thermal photonics presents a unique set of challenges as materials need to be stable in these extreme environments and, in some cases, access higher energy polaritonic resonances commensurate with energy densities of a blackbody at higher temperatures.

Since Rubio et al's prediction in 1994,[7] the potential of boron nitride nanotubes (BNNTs) and its two-dimensional (2D) counterpart, hexagonal boron nitride (hBN), has spread to many scientific communities because of their unique set of properties such as high thermal conductivity, thermal stability, mechanical strength, and neutron absorption.[8−10] This combination of properties makes BNNTs appealing for many applications in the aerospace industry, among others, where materials need to routinely sustain extreme environmental conditions. The past decade has also seen the materials make waves in the fields of nanophotonics and quantum optics due to their ability to support phonon polaritons[11,12] and behave as single photon emitters.[13,14]

Plasmonic metamaterials[2,15−19] have been proposed as systems for controlling radiative thermal emission. One specific design that has been experimentally demonstrated for thermophotovoltaic applications is epsilon-near-zero thermal metamaterials.[2,15,16] However, the high-loss and low melting point of metals reduces the choice of materials available for such thermal metamaterials. Polar dielectric materials support-

ing phonon polaritons have also been investigated with great success[20-24] but these materials are limited to low frequency mid-IR optical phonons <1200 cm^{-1} (>8.6 μm). Interestingly, hBN is a natural hyperbolic material that has shown thermal stability at temperatures up to 1173 K.[8] The combination of thermal stability, low-loss, and hyperbolic permittivity of hBN and BNNTs make them excellent candidates for high-temperature infrared photonics.

It is important to note that we choose boron nitride for three fundamental reasons: (1) It is a high-temperature ceramic with temperature stability greater than 1000 K. (2) The phonon polaritons can be excited thermally and present an important degree of freedom for radiative heat transfer applications. (3) It is extremely challenging to find polaritonic ceramics with high-frequency optical phonon excitations. This aspect is necessary for practical applications where the blackbody spectrum is shifted closer to the near-infrared as opposed to the conventional mid-infrared curve at room temperature. For comparison, the phonon−polariton frequencies of other materials such as silicon carbide are lower and mostly lie in the mid-infrared range from 10 to 20 μm (see Table 1). In this

Table 1. Optical Phonon Frequencies of Common Phonon Polaritonic Materials[a]

material permittivity	ω_{LO} (λ_{LO}) [cm^{-1}] (μm)	ω_{TO} (λ_{TO}) [cm^{-1}] (μm)	γ [cm^{-1}]	ε_∞	ref
hBN ($\varepsilon_\parallel/\varepsilon_{t,a}$)	1614 (6.20)	1360 (7.35)	7	4.90	11
hBN ($\varepsilon_\perp/\varepsilon_r$)	825 (12.12)	760 (13.16)	2	6.76	11
cBN	1340 (7.46)	1065 (9.39)	40.5	4.5	26
SiO$_2$	1186 (8.43)	1167 (8.57)	4.43		27
	1112 (9.00)	1046 (9.56)	15.53		
	1106 (9.04)	1058 (9.45)	0.42	2.09	
	814 (12.29)	799 (12.52)	12.94		
	525 (19.05)	434 (23.04)	54.14		
SiC	969 (10.32)	793 (12.61)	4.76	6.70	28
SrTiO$_3$	788 (12.69)	543 (18.42)	17.0		29−31
	474 (21.10)	175 (57.14)	5.4	5.10	
	172 (58.14)	91 (109.89)	15.0		
α-GaN	740 (13.51)	530 (18.87)	7	5.40	32
β-GaN	739 (13.53)	553 (18.08)	7	5.35	32
GaP	403 (24.8)	367 (27.25)	1.29	9.09	33

[a]Materials show that the in-plane optical phonons of hBN have the highest frequencies.

study, we specifically look at the radiative thermal emission spectrum of a disordered system of BNNT nanoantennas. This nanotube geometry is required becuase hyperbolic modes are dark modes with a large wavevector, which cannot escape a flat thin film. We show direct measurement of the stable thermal emission at high temperatures in agreement with theory of hyperbolic Reststrahlen bands. Our work paves the way for high-temperature thermal photonics with BNNTs.

hBN is a 2D material that has the same hexagonal crystal structure as graphene but with alternating boron and nitrogen atoms in place of carbon. These 2D layers can be stacked on top of each other to form bulk hBN. Optically, this polymorph forms an extremely anisotropic material with the perpendicular ($\varepsilon_\perp$) and parallel ($\varepsilon_\parallel$) components of permittivity well modeled as Lorentz oscillators

$$\varepsilon(\omega) = \varepsilon' + i\varepsilon'' = \varepsilon_\infty\left(1 + \frac{\omega_{LO}^2 - \omega_{TO}^2}{\omega_{TO}^2 - \omega^2 - i\omega\gamma}\right) \quad (1)$$

In this Lorentz model, ω is the frequency of the incident radiation; ε_∞ is the high (infinite) frequency limit of permittivity; ω_{LO} and ω_{TO} are the resonance frequencies of the longitudinal and transverse optical phonons, respectively; γ is the damping parameter.

We know that the resonant frequency of a Lorentz oscillator is inversely proportional to the square root of the mass of the oscillator ($\omega_{TO} \propto 1/\sqrt{m}$). Because boron and nitrogen are among the lightest elements capable of forming polar crystals, hBN and BNNTs produce the highest known optical phonon frequencies. Table 1 shows the optical phonon frequencies used to model the perpendicular ($\varepsilon_\perp$) and parallel ($\varepsilon_\parallel$) components of permittivity for hBN as well as other commonly used materials with optical phonons. All other listed materials possess lower frequency optical phonons than the in-plane phonons of hBN ($\varepsilon_\parallel$). Interestingly, because both components of permittivity have a spectrally distinct Reststrahlen band, hBN possesses both types of optical hyperbolicity. Type I, which has one negative component and two positive components ($\varepsilon_\perp' < 0$ and $\varepsilon_\parallel' > 0$), exists between 760 and 825 cm^{-1} and Type II, which has two negative components and one positive component ($\varepsilon_\perp' > 0$ and $\varepsilon_\parallel' < 0$), exists between 1360 and 1614 cm^{-1}.[25] Figure 1a shows the permittivity of both components highlighting the two Reststrahlen bands (regions of hyperbolicity).

The hyperbolic topology of the isofrequency surface of hBN leads to a large local density of states (LDOS) in hBN as a 2D material. This is due to the unbounded nature of a hyperboloid, which is in contrast to isotropic materials that possess bounded isofrequency contours of spherical or ellipsoidal topology.[34,35] One can calculate the LDOS in the near-field above a surface of hBN.[36−38] Figure 1b shows the LDOS at several near-field distances above an hBN−vacuum interface. Both Reststrahlen bands show large LDOS in the extreme near-field but decay as we move away from the interface.[39] This implies that for hBN, these are dark modes that are not present in the far-field and would not produce strong thermal radiation. However, by creating subwavelength particles (BNNTs) out of phonon polaritonic materials (hBN) we can introduce a mechanism to couple the dark modes to radiation in the far-field.

By rolling a sheet of hBN in to a tubular geometry we can form BNNTs (Figure 2), which are analogous to their carbon counterpart carbon nanotubes (CNTs). In doing so, we form an extremely anisotropic nanotube who's axial (and tangential) permittivity is equivalent to the parallel component of hBN ($\varepsilon_\parallel \to \varepsilon_{t,a}$) and who's radial permittivity is equivalent to the perpendicular component of hBN ($\varepsilon_\perp \to \varepsilon_r$). Figure 2a−d shows the orientation of permittivities for hBN and BNNTs and the atomic crystal structure of the two. Figure 2e shows an SEM image of the disordered nanotube system.

Optical Phonons in BNNTs. Mie theory is used to calculate the absorption resonances present in BNNTs. Figure 3a shows the absorption efficiency of an infinitely long isotropic cylinder for the two permittivities of hBN.[40,41] There are three resonant polaritonic modes that lead to strong absorption. First, at 1573 cm^{-1} is the tangential (T) mode that results from B—N stretching in the tangential direction (ε_t).[42,43] The second, at 1356 cm^{-1}, is the longitudinal (L)
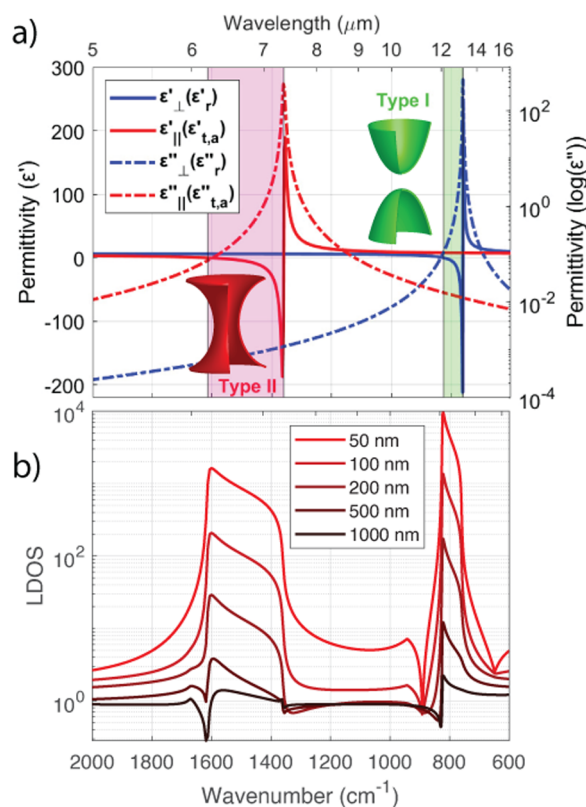
Figure 1. (a) Real (solid) and imaginary (dashed) parts of the dielectric permittivity for hexagonal boron nitride in the perpendicular (blue) and parralel (red) directions. For the cylindrical geometry of a nanotube, the perpendicular component becomes radial ($\varepsilon_\perp = \varepsilon_r$) and the parallel component becomes the axial ($\varepsilon_\parallel = \varepsilon_a$) and tangential ($\varepsilon_\parallel = \varepsilon_t$) component of permittivity for a BNNT. The two Reststrahlen bands are highlighted in magenta (upper band) and green (lower band). (b) LDOS above an hBN−vacuum interface at various distances from 50 nm (top) to 1000 nm (bottom).
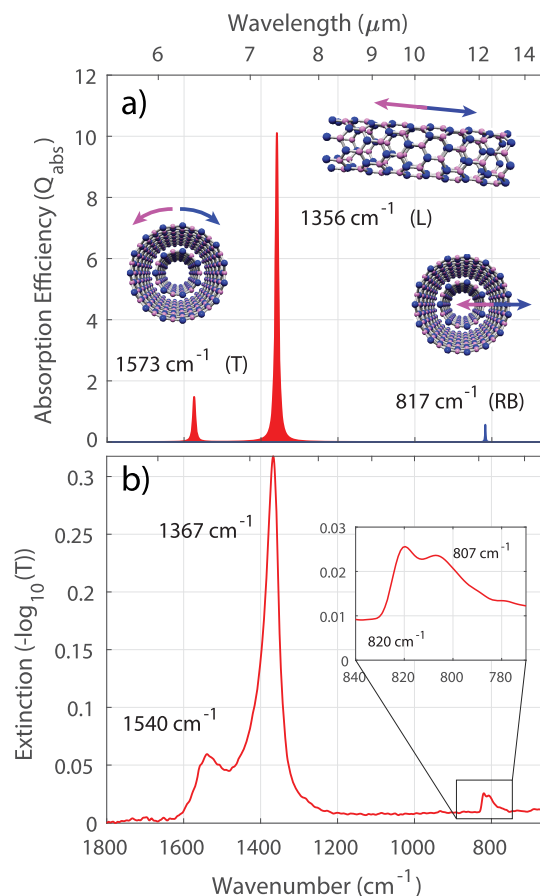

Figure 3. (a) Absorption efficiency for an infinitely long cylindrical hBN nanotube. The T and L modes correspond to the upper frequency oscillator ($\varepsilon_{t,a}$) and are shown in red, while the RB mode corresponds to the lower frequency oscillator (ε_r) is shown in blue. Schematics of each mode are shown and illustrate the boron (pink) and nitrogen (blue) ion movement for a given incident field. (b) Extinction spectrum for the disordered system of BNNTs.

mode and results from B—N stretching in the axial direction (ε_a).[42,43] Third is the radial buckling (RB) mode at 817 cm^{-1} which is the result of B—N oscillations between tubes of multiwalled BNNTs (sheets of hBN) in the radial direction (ε_r).[42] These phonon polaritonic modes are analogous to modes in plasmonic nanowire systems that are common in

metamaterials and other studies.[15] Additional discussion on the resonant polaritonic modes on BNNTs can be found in the Supporting Information.

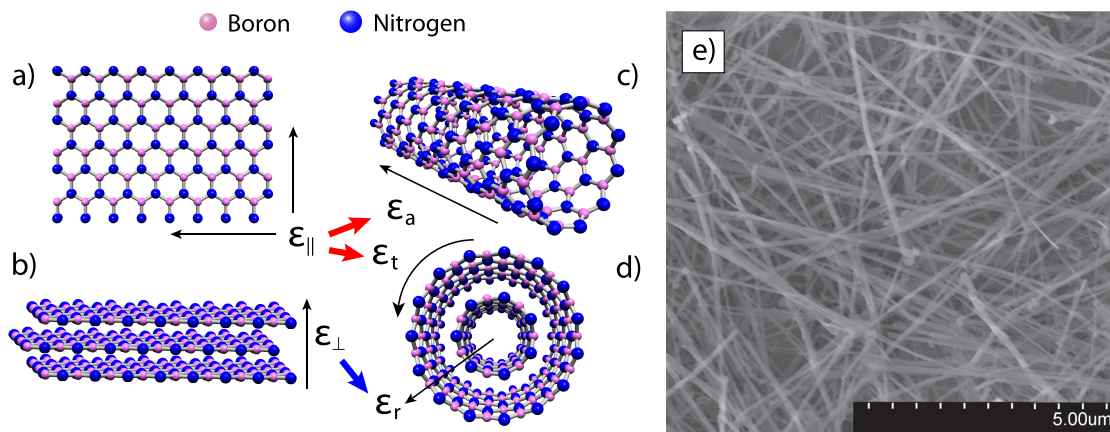IR transmission measurements are performed to confirm the presence of the predicted absorption resonances. To do this,

Figure 2. Schematic of the atomic structure of hBN from (a) plane view showing $\varepsilon_\parallel$ and (b) side view of bulk hBN showing $\varepsilon_\perp$. (c) Side view of BNNT showing ε_a and (d) end view of BNNT showing ε_r and ε_t. (e) SEM image of disordered BNNT system from which transmission and emission measurements are taken.

multiwalled BNNTs of an average diameter of 50 nm and lengths of 5−20 μm are dispersed on to a polished Si wafer that is partially transmissive from 4 to 25 μm. The transmission measurement is plotted as the extinction spectrum $(-\log_{10}(T))$ and is shown in Figure 3b).

Figure 3b clearly shows the three absorption resonances predicted by Mie theory in Figure 3a. The L mode occurs at 1367 cm^{-1} which we consider to be a negligible shift from 1356 cm^{-1}. The T mode is now located at 1540 cm^{-1}, a 33 cm^{-1} shift from predicted. This is likely due to the overlapping of T and L mode peaks as well as a shift in the optical phonon frequencies caused by the curvature of the nanotube geometry, which is supported by other studies that observe a shift in the frequency of this mode for varying nanotube radii.[43] Note that because multiwalled nanotubes are used in our experiment, there are a large number of inner tubes with relatively small diameters (e.g., 5 nm). These small inner tubes would cause noticeable shifts as predicted by Wirtz et al.[42] This would also suggest that for disordered systems of BNNTs with varying radii, a slight broadening of this mode should be observed, as is seen here. Because the T and L mode peaks are spectrally close, the broadening would result in an overlap of these two modes. The overlap and interaction of the broadened modes also contributes to the perceived peak shifting. A sharper T mode emission peak should be possible with precise control over nanotube radii. Interestingly, the weak RB mode appears to have split into two peaks located at 807 and 820 cm^{-1}. Although this "splitting" has been observed before in other BNNT studies,[43] the origin is not well understood. Further calculations from first-principles are needed to identify the cause but speculatively it could be the result of complex interaction between multiple layers of a multiwalled BNNT with different chiralities.[43]

Thermal Emission Spectroscopy. Kirchoff's law states that the linear spectral and angular emissivity $(\epsilon(\omega,\theta))$ is equal to the spectral and angular absorptivity $(\alpha(\omega,\theta))$.[44] This suggests that strong absorption bands should manifest themselves in thermal emission. The emission enhancement occurs due to the hyperbolic polariton modes in the Reststrahlen band of hBN. By heating the sample up to high temperatures, we are thermally populating these polaritonic modes. The polaritonic nature of these modes along with nanotubular structure allows coupling to electromagnetic fields and enables strong thermal radiation.

Thermal emission measurements are performed with a custom high-temperature vacuum chamber IR spectroscopy set up shown in Figure S1 and described in more detail in Supporting Information and ref 24. To isolate thermal emission from the BNNTs one must suppress background thermal radiation generated by the substrate heater. To achieve this, the disordered BNNT system is deposited on a refractory high IR reflectivity thin film (300 nm of tungsten). Figure 4 shows the emissivity spectrum of the disordered BNNT system on a 300 nm tungsten thin film at 938 K.

The emissivity spectrum is calculated as

$$\epsilon(\omega, \theta, T_S) = \frac{S_S(\omega, \theta, T_S) - S_R(\omega, T_R)}{L(\omega, T_S)R_{det}(\omega)A_{spot}\Omega} \quad (2)$$

where $S_S(\omega,\theta,T_S)$ is the spectral angular radiance of the sample at temperature T_S and angle θ, $S_R(\omega,T_R)$ is the background spectral radiance of the room and optical elements in the beam path at room temperature, $L(\omega,T_S)$ is the spectral radiance of a
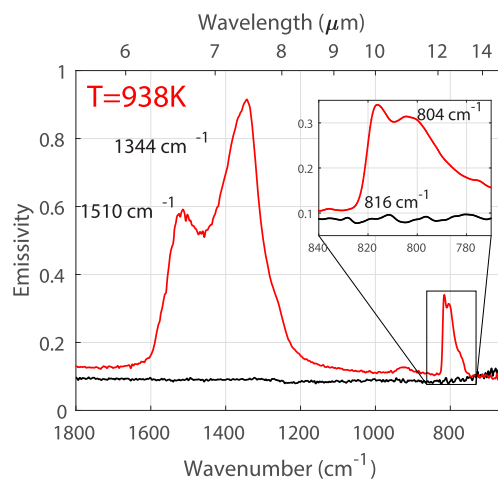

Figure 4. Spectral emissivity of BNNT system on tungsten thin film (solid red) at 938 K. The emissivity spectrum of a tungsten thin film is shown (solid black) for reference.

blackbody at temperature T_S, $R_{det}(\omega)$ is the calibrated responsivity function of the detector, A_{spot} is the collection spot size on the sample and Ω is the solid angle of collection.

In the emissivity spectrum we see the three spectrally distinct absorption bands common to the Mie absorption efficiency (Figure 3a)) and extinction spectra (Figure 3b)). The T and L modes now exist at 1510 and 1344 cm^{-1} respectively. The "splitting" of the RB mode is still observed in emission measurement and are now located at 803 and 814 cm^{-1}. This red shifting of optical phonon modes is discussed in the following section.

Temperature Dependence of Spectral Emissivity. To characterize the red shift of the absorption bands at elevated temperatures, we measure emissivity from 560 to 938 K. Figure 5 shows the emissivity spectrum over this temperature range,
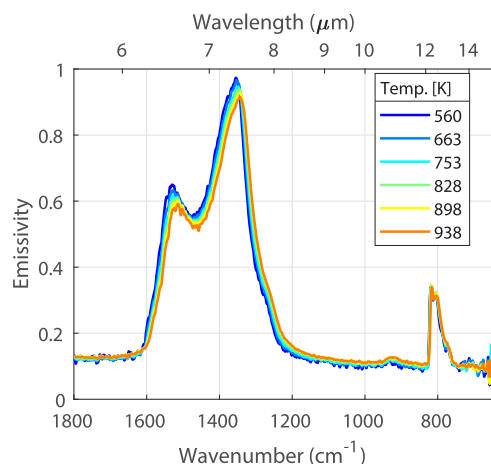

Figure 5. Temperature dependence of BNNT emissivity.

where we observe a frequency shift of ~18 cm^{-1} for the T mode and ~13 cm^{-1} for the L mode. This is the result of red shifting of optical phonon frequencies of hBN at elevated temperatures[24] likely caused by thermal expansion. We note that the shift in the RB mode appears to be less pronounced, now occurring at 803 and 814 cm^{-1}. However, if you analyze the peak shifting in terms of wavelength, all modes shift by ~50 nm over the full temperature range (560−938 K). Also of

note is that for more moderate temperatures (560 K), the L mode peak approaches the blackbody limit achieving an emissivity of $\varepsilon = 0.97$. This is due to increased polaritonic damping at higher temperatures. The temperature dependence of the emissivity spectrum reveals the shift of polaritonic properties of hBN at elevated temperatures. This is consistent with previous studies of the temperature dependent emission of other polar dielectrics like SiC.[24,45]

Thermal Antenna Effect in Disordered Nanotubes. In general, a disordered system of particles such as this should exhibit no angularly dependent emission behavior. However, for our system, there is one degree of quasi-order, which is that the nanotubes are predominantly lying down with their axis parallel to the substrate plane. Using this fact, we can take polarized angularly dependent thermal emission measurements to further probe and experimentally distinguish the optical phonon modes of BNNTs. Because the L mode results from ion oscillations along the nanotube length, the radiation emitted from this mode will be polarized along the nanotube axis. Figure 6 shows the two basis orientations that a nanotube
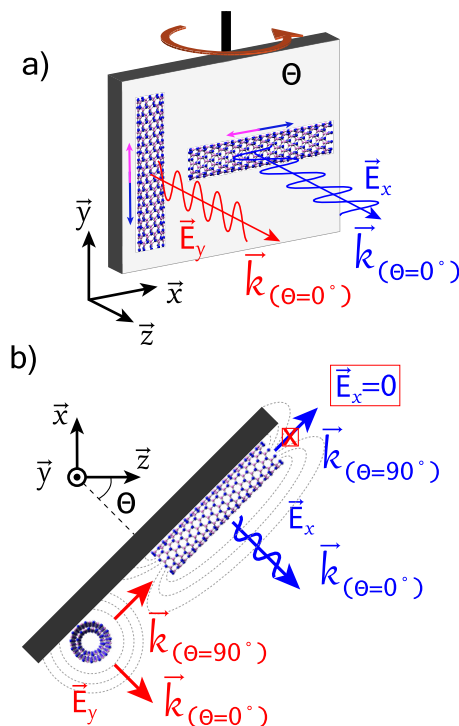
a)

b)

Figure 6. Schematic of the L mode radiation pattern and polarization orientation. Emission is measured in the z-direction. (a) An oblique angle schematic with polarization state of the L mode emitted normal to the sample from two orthogonally oriented nanotubes. (b) Top down view of the same two oriented nanotubes at angle θ. Due to the antenna effect of thermal radiation, there is no $\vec{E}_x$ emission at $\theta = 90°$ for the L mode.

can have and the electric field polarization for each. If we consider each nanotube as a dipole antenna, we know that the radiation pattern is strongest when the wave vector is perpendicular to the nanotube axis ($\vec{k} \perp \vec{l}_c$) and does not radiate parallel to the nanotube axis ($\vec{k} \parallel \vec{l}_c$). We can therefore attempt to remove the L mode resonance from the emissivity spectrum by collecting emission at highly oblique angles ($\theta \rightarrow$

90°) to suppress $\vec{E}_x$ polarized emission and use a wire grid IR polarizer to remove $\vec{E}_y$ polarized emission.

Figure 7 shows the x-polarized emissivity spectrum as the angle is varied from $\theta = 0-70°$. Here, the BNNTs behave as
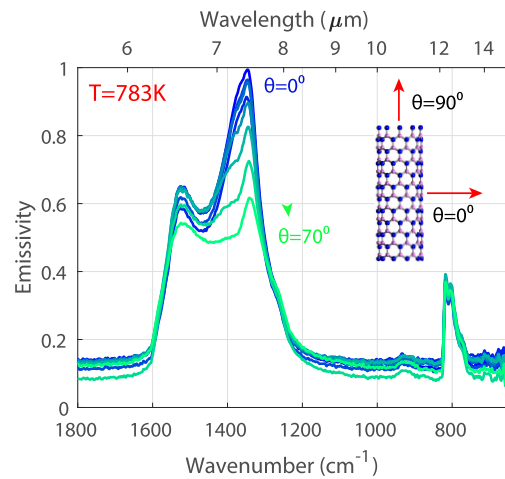
Figure 7. Angular dependence of $\vec{E}_x$ polarized BNNT emissivity at 783 K.

nanoantennas where the heat driven fluctuating dipole moments in optically active phonons lead to far-field thermal radiation. We can see the main L mode peak is suppressed at higher angles, whereas the other modes (T and RB) are largely unchanged. If precise control over the orientation of the BNNT system was possible, we would be able to more effectively suppress the L mode leaving only the T and RB mode present in the emissivity spectrum. The relative presence of the L mode is an indication that for our sample, some BNNTs are not purely in the plane of the substrate and have a slight angle relative to the substrate surface. Also, our experimental setup limits us from reaching measurements closer to 90°.

In summary, we have measured the emissivity spectrum of a disordered BNNT system and show that its thermal antenna behavior can be observed even in a disordered system. Three emission bands located at 1510, 1344, and 810 cm^{-1} (6.6, 7.4, and 12.3 μm) are present in the emissivity spectrum (at 938 K), which are the result of optical phonon modes supported by BNNTs. The emissivity spectrum is compared to the measured extinction spectrum and Mie absorption efficiency and show strong agreement. At normal incidence, the emissivity of the L mode approaches the blackbody limit ($\epsilon = 0.97$ at 560 K).

We would like to highlight that due to the low mass of boron and nitrogen atoms, hBN possesses the highest known optical phonon frequencies. Moreover, although the hBN LO frequency is generally not observed in planar forms of the material, it is present in the tubular form of BNNTs. To our knowledge, the T mode present in the emissivity spectrum of our BNNT system is the highest frequency thermal polariton mode ever measured, making it an excellent candidate for high-temperature thermal photonics.

A proposed system that would isolate the emission of this T mode from its neighboring L mode is a forest of vertically standing BNNTs. This can be synthesized via a recently developed catalytic chemical vapor deposition (CCVD) technique, where specific active catalysts (like MgO, Ni, and Fe) are first deposited on desired substrates and the BNNT

forest can then be grown on the substrates in tube furnaces.[46−48] In such a device, the L mode emission would radiate parallel to the samples plane with the T and RB modes propagating normal to the sample ($\theta = 0°$). Figure 8 shows the theoretical absorption/emission efficiency of this proposed system at normal incidence.
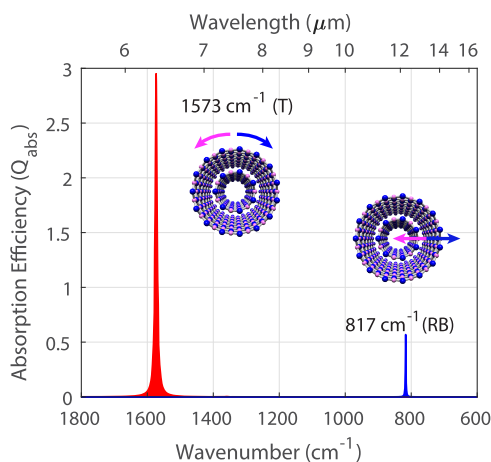

Figure 8. Theoretical absorption efficiency of vertically aligned BNNT forest.

With interest in BNNTs expanding, we believe these results will help advance thermal photonics, especially for researchers exploring the potential of this exciting material for extreme environment and high-temperature applications. The distinct thermal emission spectrum and characteristic antenna effects of BNNTs make them an appealing candidate for many thermal photonics applications. For example, very compact on-chip quasi-coherent sources may potentially be achieved with BNNTs. In optical sensing or spectroscopy systems, where infrared sources are required, BNNTs can be integrated to provide narrow-band and directional thermal light emission. For applications such as thermophotovoltaic emitters and radiative cooling coatings, the spectral peaks of boron nitride nanotubes have to be tailored into appropriate spectral bands.

ASSOCIATED CONTENT

Ⓢ Supporting Information

The Supporting Information is available free of charge on the ACS Publications website at DOI: 10.1021/acs.nanolett.9b03059.

Details on calculations and experimental methods (PDF)

AUTHOR INFORMATION

Corresponding Author
*E-mail: zjacob@purdue.edu.

ORCID Ⓘ
Xueji Wang: 0000-0002-0006-4050
Sandipan Pramanik: 0000-0001-6761-4734
Zubin Jacob: 0000-0002-7009-2065

Notes
The authors declare no competing financial interest.

REFERENCES

(1) Molesky, S.; Dewalt, C. J.; Jacob, Z. *Opt. Express* **2013**, *21*, A96−A110.
(2) Dyachenko, P. N.; Molesky, S.; Petrov, A. Y.; Störmer, M.; Krekeler, T.; Lang, S.; Ritter, M.; Jacob, Z.; Eich, M. *Nat. Commun.* **2016**, *7*, 11809.
(3) Rephaeli, E.; Fan, S. *Opt. Express* **2009**, *17*, 15145−15159.
(4) Rinnerbauer, V.; Lenert, A.; Bierman, D. M.; Yeng, Y. X.; Chan, W. R.; Geil, R. D.; Senkevich, J. J.; Joannopoulos, J. D.; Wang, E. N.; Soljai, M.; Celanovic, I. *Adv. Energy Mater.* **2014**, *4*, 1400334.
(5) Raman, A. P.; Anoma, M. A.; Zhu, L.; Rephaeli, E.; Fan, S. *Nature* **2014**, *515*, 540.
(6) Zhai, Y.; Ma, Y.; David, S. N.; Zhao, D.; Lou, R.; Tan, G.; Yang, R.; Yin, X. *Science* **2017**, *355*, 1062−1066.
(7) Rubio, A.; Corkill, J. L.; Cohen, M. L. *Phys. Rev. B: Condens. Matter Mater. Phys.* **1994**, *49*, 5081−5084.
(8) Zhi, C.; Bando, Y.; Tang, C.; Golberg, D. *Mater. Sci. Eng., R* **2010**, *70*, 92−111.
(9) Jiang, P.; Qian, X.; Yang, R.; Lindsay, L. *Phys. Rev. Materials* **2018**, *2*, 064005.
(10) Chang, C. W.; Fennimore, A. M.; Afanasiev, A.; Okawa, D.; Ikuno, T.; Garcia, H.; Li, D.; Majumdar, A.; Zettl, A. *Phys. Rev. Lett.* **2006**, *97*, 085901.
(11) Caldwell, J. D.; Kretinin, A. V.; Chen, Y.; Giannini, V.; Fogler, M. M.; Francescato, Y.; Ellis, C. T.; Tischler, J. G.; Woods, C. R.; Giles, A. J.; Hong, M.; Watanabe, K.; Taniguchi, T.; Maier, S. A.; Novoselov, K. S. *Nat. Commun.* **2014**, *5*, 5221.
(12) Xu, X. G.; Ghamsari, B. G.; Jiang, J.-H.; Gilburd, L.; Andreev, G. O.; Zhi, C.; Bando, Y.; Golberg, D.; Berini, P.; Walker, G. C. *Nat. Commun.* **2014**, *5*, 4782.
(13) Ahn, J.; Xu, Z.; Bang, J.; Allcca, A. E. L.; Chen, Y. P.; Li, T. *Opt. Lett.* **2018**, *43*, 3778−3781.
(14) Tran, T. T.; Elbadawi, C.; Totonjian, D.; Lobo, C. J.; Grosso, G.; Moon, H.; Englund, D. R.; Ford, M. J.; Aharonovich, I.; Toth, M. *ACS Nano* **2016**, *10*, 7331−7338.
(15) Starko-Bowes, R.; Atkinson, J.; Newman, W.; Hu, H.; Kallos, T.; Palikaras, G.; Fedosejevs, R.; Pramanik, S.; Jacob, Z. *J. Opt. Soc. Am. B* **2015**, *32*, 2074−2080.
(16) Pendharker, S.; Hu, H.; Molesky, S.; Starko-Bowes, R.; Poursoti, Z.; Pramanik, S.; Nazemifard, N.; Fedosejevs, R.; Thundat, T.; Jacob, Z. *J. Opt.* **2017**, *19*, 055101.
(17) Lee, B. J.; Fu, C. J.; Zhang, Z. M. *Appl. Phys. Lett.* **2005**, *87*, 071904.
(18) Liu, N.; Mesch, M.; Weiss, T.; Hentschel, M.; Giessen, H. *Nano Lett.* **2010**, *10*, 2342−2348.
(19) Bagheri, S.; Zgrabik, C. M.; Gissibl, T.; Tittl, A.; Sterl, F.; Walter, R.; De Zuani, S.; Berrier, A.; Stauden, T.; Richter, G.; Hu, E. L.; Giessen, H. *Opt. Mater. Express* **2015**, *5*, 2625−2633.
(20) Schuller, J. A.; Taubner, T.; Brongersma, M. L. *Nat. Photonics* **2009**, *3*, 658−661.
(21) Greffet, J.-J.; Carminati, R.; Joulain, K.; Mulet, J.-P.; Mainguy, S.; Chen, Y. *Nature* **2002**, *416*, 61−64.
(22) Dahan, N.; Niv, A.; Biener, G.; Gorodetski, Y.; Kleiner, V.; Hasman, E. *J. Heat Transfer* **2008**, *130*, 112401.
(23) Caldwell, J. D.; Lindsay, L.; Giannini, V.; Vurgaftman, I.; Reinecke, T. L.; Maier, S. A.; Glembocki, O. J. *Nanophotonics* **2015**, *4*, 44−68.
(24) Starko-Bowes, R.; Dai, J.; Newman, W.; Molesky, S.; Qi, L.; Satija, A.; Tsui, Y.; Gupta, M.; Fedosejevs, R.; Pramanik, S.; Xuan, Y.; Jacob, Z. *J. Quant. Spectrosc. Radiat. Transfer* **2018**, *216*, 99−104.
(25) Shekhar, P.; Atkinson, J.; Jacob, Z. *Nano Convergence* **2014**, *1*, 14.
(26) Gielisse, P. J.; Mitra, S. S.; Plendl, J. N.; Griffis, R. D.; Mansur, L. C.; Marshall, R.; Pascoe, E. A. *Phys. Rev.* **1967**, *155*, 1039−1046.

(27) Kischkat, J.; Peters, S.; Gruska, B.; Semtsiv, M.; Chashnikova, M.; Klinkmüller, M.; Fedosenko, O.; Machulik, S.; Aleksandrova, A.; Monastyrskyi, G.; Flores, Y.; Masselink, W. T. *Appl. Opt.* **2012**, *51*, 6789−6798.

(28) Arnold, C.; Marquier, F. m. c.; Garin, M.; Pardo, F.; Collin, S.; Bardou, N.; Pelouard, J.-L.; Greffet, J.-J. *Phys. Rev. B: Condens. Matter Mater. Phys.* **2012**, *86*, 035316.

(29) Vogt, H.; Rossbroich, G. *Phys. Rev. B: Condens. Matter Mater. Phys.* **1981**, *24*, 3086−3091.

(30) Kamaras, K.; Barth, K.; Keilmann, F.; Henn, R.; Reedyk, M.; Thomsen, C.; Cardona, M.; Kircher, J.; Richards, P. L.; Stehl, J. *J. Appl. Phys.* **1995**, *78*, 1235−1240.

(31) Gervais, F. Strontium Titanate ($SrTiO_3$). In *Handbook of Optical Constants of Solids*; Palik, E. D., Ed.; Academic Press: Boston, 1998.

(32) Shkerdin, G.; Rabbaa, S.; Stiens, J.; Vounckx, R. *J. Phys. D: Appl. Phys.* **2012**, *45*, 495103.

(33) Marschall, N.; Fischer, B. *Phys. Rev. Lett.* **1972**, *28*, 811−813.

(34) Jacob, Z. *Nat. Mater.* **2014**, *13*, 1081.

(35) Poddubny, A.; Iorsh, I.; Belov, P.; Kivshar, Y. *Nat. Photonics* **2013**, *7*, 948.

(36) Molesky, S.; Jacob, Z. *Phys. Rev. A: At., Mol., Opt. Phys.* **2019**, *99*, 033833.

(37) Cortes, C. L.; Newman, W.; Molesky, S.; Jacob, Z. *J. Opt.* **2012**, *14*, 063001.

(38) Guo, Y.; Cortes, C. L.; Molesky, S.; Jacob, Z. *Appl. Phys. Lett.* **2012**, *101*, 131106.

(39) Phillips, C.; Gilburd, L.; Xu, X. G.; Walker, G. C. *J. Phys. Chem. Lett.* **2019**, *10*, 4851−4856.

(40) Kerker, M. *The scattering of light and other electromagnetic radiation*; Academic Press, 1969.

(41) Bohren, C. F.; Huffman, D. *Absorption and scattering of light by small particles*; Wiley Science, 1983.

(42) Wirtz, L.; Rubio, A.; de la Concha, R. A.; Loiseau, A. *Phys. Rev. B: Condens. Matter Mater. Phys.* **2003**, *68*, 045425.

(43) Lee, C. H.; Wang, J.; Kayatsha, V. K.; Huang, J. Y.; Yap, Y. K. *Nanotechnology* **2008**, *19*, 455605.

(44) Greffet, J.-J.; Nieto-Vesperinas, M. *J. Opt. Soc. Am. A* **1998**, *15*, 2735−2744.

(45) Herve, A.; Drevillon, J.; Ezzahri, Y.; Joulain, K.; Meneses, D.; Hugonin, J.-P. *J. Quant. Spectrosc. Radiat. Transfer* **2016**, *180*, 29−38.

(46) Ahmad, P.; Khandaker, M. U.; Amin, Y. M. *Mater. Manuf. Processes* **2015**, *30*, 706−710.

(47) Lee, C. H.; Xie, M.; Kayastha, V.; Wang, J.; Yap, Y. K. *Chem. Mater.* **2010**, *22*, 1782−1787.

(48) Belkerk, B. E.; Achour, A.; Zhang, D.; Sahli, S.; Djouadi, M.-A.; Yap, Y. K. *Appl. Phys. Express* **2016**, *9*, 075002.